Journal of Environmental Radioactivity 259-260 (2023) 107118

Contents lists available at ScienceDirect

Journal of Environmental Radioactivity

journal homepage: www.elsevier.com/locate/jenvrad

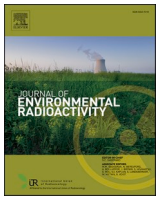

Estimating geothermal and background radiation hotspots from primordial radionuclide concentrations in geology of South Africa

Jacques Bezuidenhout

Faculty of Military Science, Stellenbosch University, South Africa

ARTICLE INFO

Keywords:
Naturally occurring radionuclides
Geology
Background radiation
Thermal hotspots
QGIS
South Africa

ABSTRACT

Naturally occurring radionuclides are the main generator of geothermal energy in the Earth's crust and mantle. The generated energy is consequently directly proportional to the concentrations of the three main naturally occurring radionuclides (uranium, thorium and potassium), which are primordial in origin. Concentrations of these naturally occurring radionuclides were extracted for all the different geological rock units in South Africa. The radionuclide concentrations were then mapped and integrated by using QGIS. The results were used to estimate and map the geothermal energy production rates for the rock units. The radionuclide concentrations in the rock units were also used to identify regions with high radiation background. These radiation hotspots were plotted and investigated. The estimated geothermal energy and background radiation hotspots were compared to measurements and projections of other studies and good corelations were found.

1. Introduction

Primordial nuclides which produce geothermal energy occur naturally in the crust, mantle, and core of the Earth (Ruedas, 2017). The geothermal energy is mainly produced by the radioactive decay of potassium (^{40}K), uranium (^{238}U) and thorium (^{232}Th), all with half-lives in the order of the age of the Earth. The friction between the edges of the continental plates also produces a small amount of geothermal energy, but the contribution of this was omitted in this study due to South Africa being well clear of the edges of the African continental plate (Morgan, 1989). The geothermal energy results in various heated surface phenomena like geysers and hot springs. Geothermal energy is available in varying amounts on the surface of the Earth and increases rapidly with depth (Morgan, 1989). This energy can be harvested and utilized to contribute towards the energy needs of humans. South Africa is highly dependent on coal burning power stations which have severe environmental consequences. Geothermal energy consequently provides an environmentally friendly alternative to electricity generation by coal. One of the aims of this study is to show areas where the natural potential for power generation by means of geothermal energy is high.

Humans on Earth are exposed to sources of radiation on a daily basis. Background radiation is defined as the sum of cosmic radiation, indoor and outdoor radionuclides in air, and natural radioactivity in rocks, soils, water, and food (NCRP, 2015). The global average annual effective dose that humans receive due to natural sources is 2.4 mSv/a (UNSCEAR, 2000). Terrestrial sources like natural radionuclides in rocks and soils contribute 0.48 mSv/a and, radon and thoron which are closely related to these sources contribute another 1.26 mSv/a. Natural radionuclides which produce geothermal energy consequently contribute substantially towards background radiation. This results in a close relationship between potential geothermal energy and human exposure to terrestrial background radiation. The second aim of this study is therefore to identify high terrestrial background radiation areas in South Africa.

2. Geological setting

South Africa has a diverse geology which includes greenstone and orogenic belts, cratons, impact craters and large deposits of minerals. The geology of South Africa dates to 3600 million years and consequently includes some of the oldest rocks on the planet. The relief and structure of South Africa are dominated by a stable underlining geology dating to the pre-Cambrian era. This gives rise to a central plateau with a well-defined escarp to the east, south and west. The Kaapvaal Craton which is overlaid in part by sedimentary formations forms the basement rock of this escarp (Mc Carthy and Rubidge, 2005). Fig. 1 shows a chronostratigraphic map of South Africa with the major geological features, marked A to G, that will be discussed. These areas include the exposed sections of the orogenic and greenstone belts, the largest impact crater on the globe, the Cape Fold Belt, the Drakensberg Group which

E-mail address: jb@sun.ac.za.

https://doi.org/10.1016/j.jenvrad.2023.107118
Received 28 September 2022; Received in revised form 5 January 2023; Accepted 11 January 2023
Available online 14 January 2023
0265-931X/

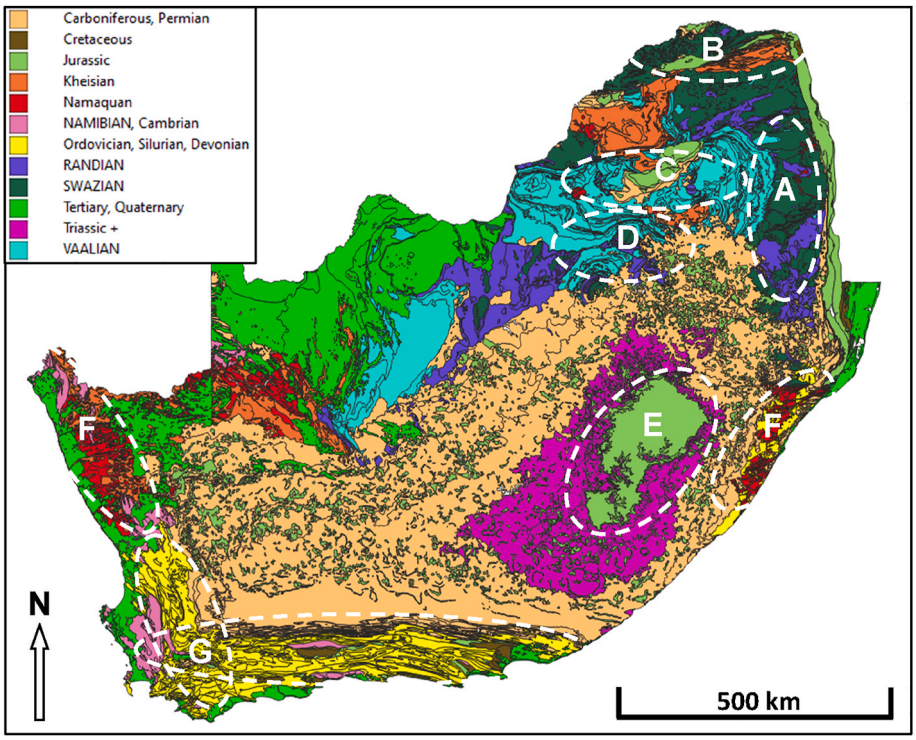

Fig. 1. A chronostratigraphic map of South Africa indicating the evolutions during the different geological periods in a colour array. The areas that are discussed below are marked from A to G. This map was adapted from a chronostratigraphic map of South Africa which was produced by the Council of Geoscience. (For interpretation of the references to colour in this figure legend, the reader is referred to the Web version of this article).

forms the highest protrusions in the country and the Bushveld Complex and Witwatersrand Basin which houses vast mineral deposits.

The Transvaal Supergroup, from the Vaalian period, which overlays the Wolfberg group forms the upper layer of the eastern part of the central plateau (area marked as A in Fig. 1). This group mainly consist of sandstone and mudstone. The exposed shale and slate of the Wolfberg group dominates most of the eastern escarp which runs from the Soutpansberg mountain in the far north to the Barberton Greenstone Belt in the south. The lowveld below the escarp is underlaid by Greenstone which is intruded by gneiss and granite (Viljoen et al., 2015).

The Limpopo Mobile Belt (area marked as B in Fig. 1) is a transboundary suite of supracrustal rocks that runs between the Kaapvaal Craton and the Zimbabwe craton to the north of that. The Belt is divided into three major zones, the Northern Zone, the Central Zone, and the Southern Zone, of which the latter two lie within South Africa. The Limpopo Mobile Belt which is dominated by high grade metamorphic rock units subsequently covers the far northern part of South Africa (Chinoda et al., 2009). The basement of the Belt in South Africa comprises of leucocratic gneiss, quartz diorite and granodiorite (Fripp, 1983). The overlaying rock units include gneisses, quartzites, amphibolite, marble and granitoids (Bahnemann, 1973; Sohnge et al., 1948).

The Bushveld Complex (area marked as C in Fig. 1) which was emplaced during the Kheisian period is the largest igneous intrusion on the planet and partly overlays the Kaapvaal Craton. The complex is positioned in the north-eastern centre of the plateau and protrudes the sedimentary Transvaal Supergroup. The Bushveld Complex contains some of the largest reserves of platinum, copper, vanadium, chromium, nickel, and titanium (Maier et al., 2013).

The Witwatersrand Basin (area marked as D in Fig. 1) is just south of the Bushveld Complex in the centre of the Kaapvaal Craton and comprises of very hard erosion resistant rock units of sedimentary origin. The Witwatersrand basin forms part of the larger Witwatersrand Supergroup and was formed during the Randian period. The basin includes quartzites, banded ironstones and marine lava deposits, punctuated with conglomerates and mudstones (Tucker et al., 2016). The Vredefort dome is a large meteor impact crater within the goldfields of the Witwatersrand basin. The crater itself has long since weathered away, but the geological structures at the centre of the impact are still evident. The structure is dominated by breccia and granophyre. The lithologies in the northern part of the Vredefort dome are migmatites and gneisses with intrusions of granodiorites and granites (Lana 2003; Hart et al., 1999).

The Drakensberg Group (area marked as E in Fig. 1) forms a large part of the eastern and southern escarp. The fragmentation of the supercontinent Gondwana caused rifting in the tectonic plates, and this led to the formation of the Drakensberg Group during the Jurassic period. The Drakensberg Group comprises of underlying sedimentary geological units with sandstones, lapilli, and pyroclastic deposits and overlying igneous units containing mainly basalt and andesite. Pipes through the Earth's crust brought basaltic and andesite to the surface causing dikes and sills which gives rise to the flood basalts of the Drakensberg Group (Lock et al., 1974). The dikes and sills are preserved throughout the Karoo Basin and have served as a weathering barrier for much of the Karoo Supergroup rocks. The Karoo Supergroup mainly consist of shales and sandstones that date from the late Carboniferous up to the early Jurassic periods (Hamilton and Finlay, 1928).

The Namaqua Natal Metamorphic and Igneous Province (area marked as F in Fig. 1) is a transboundary mobile belt which is dominated by granitic and metamorphic suites that was emplaced during the Namaquan period. The Belt runs from west to east and separates the Kaapvaal Craton and the Cape Folded Belt. In the east the Belt is divided into three distinct terranes. The Tugela Terrane, to the north-east consists of gneisses and mafic metavolcanic rock units. The Mzumbe Terrane to the south contains granitoids and supracrustal gneisses. The Margate Terrane, to the far south consist of granitoids, charnockites, gneisses and granulites (Hartnady et al., 1985; Thomas et al., 1994). The geology of the north-western part of South Africa is relatively complex and also forms part of the Namaqua-Natal Metamorphic and Igneous Province. The Richtersveld Terrane to the far north comprises of

Table 1
Concentrations of potassium, uranium, and thorium that were used to populate groups, and subgroups of rock units of South Africa's geology.

Rock types, groups, and subgroups	Potassium (%)	Uranium (ppm)	Thorium (ppm)
Acid Volcanic Rock	2.3	4.3	17.0
Amphibolite	0.6	3.5	1.2
Andesite	1.7	1.6	4.9
Anorthosite	0.1	0.2	0.1
Arenite	1.1	2.0	5.7
Basalt	0.8	0.5	9.0
Basaltic Andesite	1.2	1.3	6.9
Biotite	0.7	7.9	7.9
Biotite Granodiorite	3.4	7.9	20.8
Breccia	0.1	2.4	7.4
Calcrete	BDL	0.1	0.2
Calc-silicate rocks	0.3	0.1	0.4
Carbonatite	BDL	4.9	35.7
Charnockite	0.7	0.1	0.2
Chert	0.3	BDL	0.4
Dacite	1.8	2.5	12.8
Diamictite	2.0	4.0	12.2
Diorite	0.8	0.8	1.4
Dolerite	0.6	0.4	2.1
Dolomite	0.2	2.0	2.5
Dunite	1.9	BDL	3.3
Eclogite	0.8	3.0	9.0
Enderbite	2.3	0.4	4.0
Felsite	0.3	8.4	32.0
Foyaite	3.6	33.7	159.0
Gabbro	2.4	4.9	16.4
Gabbronorite	0.2	0.3	1.2
Glimmerite	6.7	4.0	18.7
Gneiss	6.6	12.7	65.9
Granite	3.4	6.0	20.8
Granite-Gneiss	5.0	9.4	43.3
Granodiorite	3.3	6.0	23.0
Granophyre	3.8	5.2	17.0
Granulite	BDL	0.1	BDL
Gravels	2.0	4.0	10.1
Greywackes	1.1	2.0	5.7
Harzburgite	1.1	1.0	4.0
Hornblendite	0.4	4.4	17.0
Hornfels	3.4	4.0	16.0
Ijolite	6.1	3.0	3.0
Ironstone	0.6	1.7	12.5
Jaspilite	0.1	4.0	18.3
Leucocratic granite	3.4	4.3	11.9
Limestone	0.2	2.0	2.5
Mafic rocks	0.2	4.0	18.3
Magnetite	0.1	40.7	57.8
Marine gravel and Marine sediment	2.0	4.0	10.1
Melanorite	0.1	0.1	0.3
Melilitite	1.8	2.8	10.0
Microgranite	3.1	4.0	17.0
Migmatite	4.7	0.9	1.0
Monzodiorite	2.5	8.1	33.2
Monzogranite	2.8	6.0	13.5
Monzonite	3.6	9.6	33.4
Mudstone	2.5	3.9	13.4
Nephelinite	1.8	2.8	10.0
Norite	2.9	2.1	9.6
Pegmatite	3.9	7.0	24.0
Peridotite	BDL	BDL	BDL
Phoscorite	7.5	11.2	25.0
Phyllite	0.9	2.7	7.5
Picrite	0.5	0.8	9.0
Pyroxenite	3.4	1.0	18.9
Quartz Diorite	3.8	6.9	17.6
Quartz Syenite	3.3	12.0	45.0
Quartz Schist	0.9	4.1	22.7
Quartzite	0.3	BDL	0.4
Quartz-Monzonite	3.5	12.8	58.2
Rhyolite	2.4	4.8	21.6
Sandstone	1.1	1.8	5.2
Schist	1.6	3.3	8.5
Shale	0.9	4.6	14.0
Siltstone	1.8	2.3	6.6
Slate	0.9	2.7	7.5
Syenite	3.3	12.2	41.4
Syenogranite	4.5	11.6	63.2
Tholeiite	0.3	1.4	4.4
Tholeiitic	0.8	0.5	9.0
Tinguaite	3.1	22.4	62.0
Tonalite	0.9	3.3	18.5
Trachyandesite	0.7	3.1	15.5
Trachyte	7.8	11.6	15.5
Trondhjemite	0.9	1.2	18.5
Wacke	1.1	2.0	5.7
Websterite	0.2	0.4	1.3

BDL: Below Detection Limit.

Calc-alkaline lavas and granitoids with varying amphibolite-facies (Andreoli et al., 2006). The Terranes to the south and east of the Richtersveld consist of gneisses, metavolcanics, granites and charnockites (Moore, 1989; Moore et al., 1990). The Bushmanland Complex in the southwest varies between granites gneisses, quartzites and schists.

The Cape Fold Belt is a 1300 km long fold and thrust belt from the Cambrian and Ordovician periods. This mountain belt stretches along the western and southern coastlines of South Africa (area marked as G in Fig. 1). The Cape Fold Belt which forms part of the Cape Supergroup is predominantly made up of quartzitic sandstone, mudstone, and shale (Shone and Booth, 2005). The Cape Granite Suite forms the bedrock that underlies the western part of this Belt. Granite outcrops are consequently common in the far southwestern part of South Africa.

3. Method

3.1. Naturally occurring radionuclides in rock types

The different radionuclide concentrations in rock types were obtained from various databases and articles (Andreoli et al., 2006; Bezuidenhout, 2013; DicksonScott, 1997; Ferreira et al., 2016; GEOROC database; Ielsch, 2017; Mira et al., 2020; Neumann et al., 2011; Olson and Overstreet, 1964; Opiyo, 2009; Shakotko, 2014; Smithies and Marsh, 1996; Sundal et al., 2003; Tyler, 1994; Zimmermann et al., 2011). Radionuclide concentrations in rock types differ depending on geographical location and attention was therefore given to identify samples that were taken within South Africa. The majority of the concentrations was extracted from the GEOROC database, and this library allows selection based on geographical location. A few estimates were extracted from other samples around the globe when radionuclide concentrations of rock types could not be found within the boundaries of South Africa. The nuclide concentrations for all rocks which were used are listed in Table 1.

3.2. Naturally occurring radionuclides in geological units

The average concentrations in the crust of the Earth are 2.5%, 2.7 ppm and 10.5 ppm for potassium, uranium, and thorium, respectively (Rudnick and Gao, 2003). The radionuclide concentrations directly relate to the origin of the rocks be it sedimentary, metamorphic, or igneous. In general, igneous rocks show higher concentrations of natural radionuclides than sedimentary rocks. Mafic rocks like basalts and dunites normally show low concentrations of natural radionuclides, whereas igneous felsic rocks like granites show high concentrations (Ruffell et al., 2006). Sedimentary rocks like sandstone and limestone contain low concentrations of natural radionuclides (Harmsen and de Haan, 1980). There are however sedimentary rocks like illite and kaolinite rich clays, micas, feldspars, and heavy minerals like monazite,

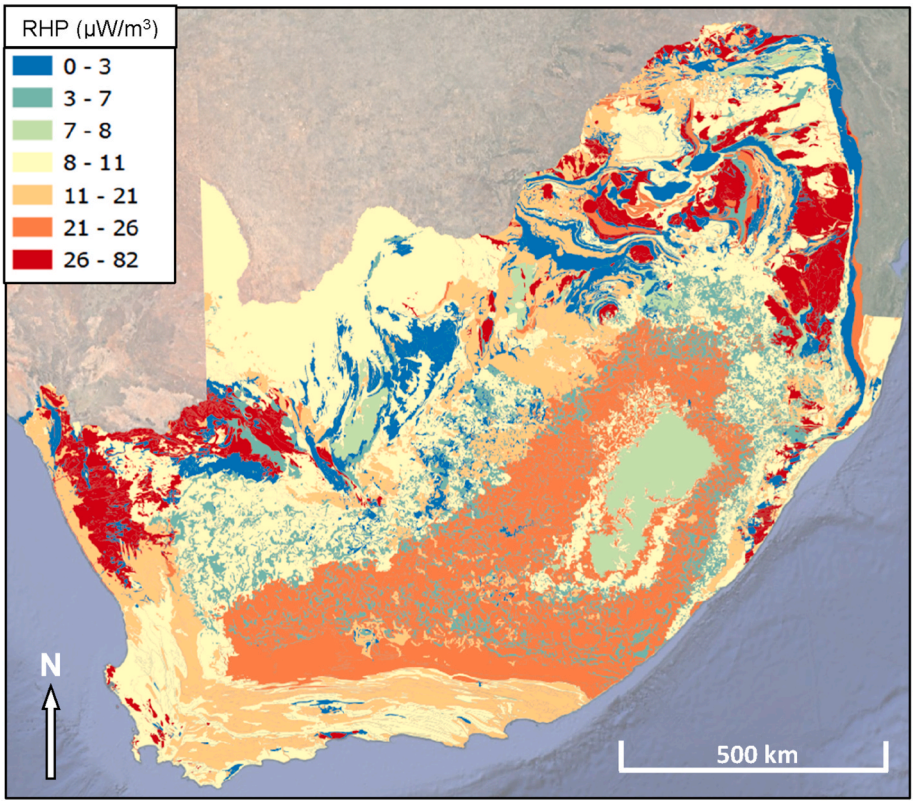

Fig. 2. A map of the estimated radioactive heat production (RHP) of each geological unit overlaid on a map of South Africa.

uraninite and thorite that display high concentrations of uranium and thorium (DicksonScott, 1997). These geophysical characteristics were used in combination with information from the geological units of South Africa to assess the occurrence of natural radionuclides in each unit.

The data of the geological units in South Africa were obtained from the Council of Geoscience of South Africa (https://www.geoscience.org.

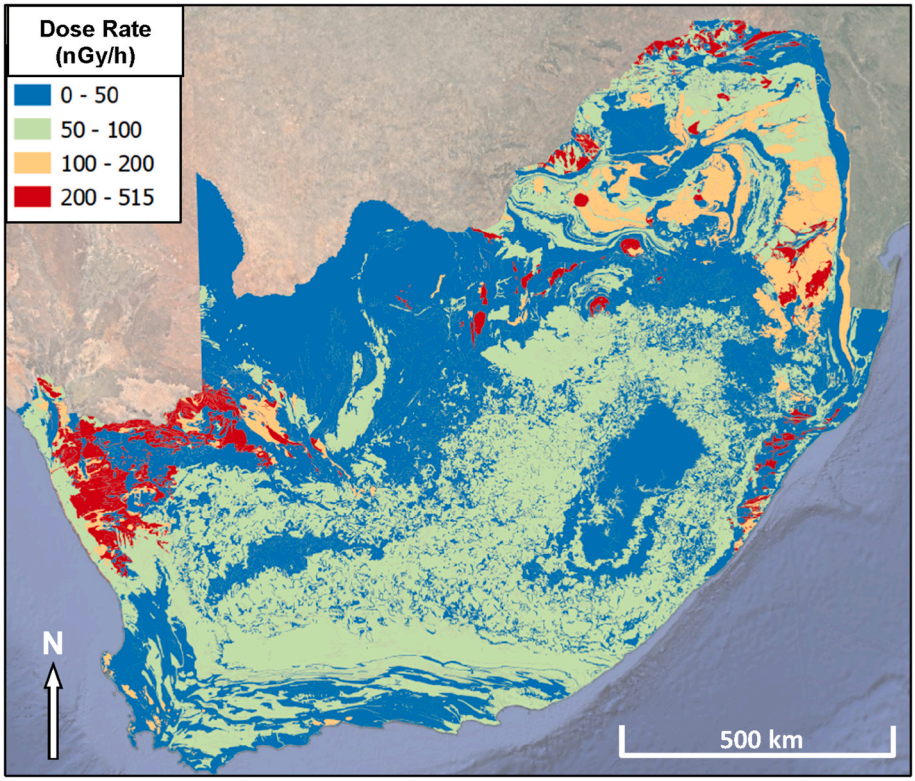

Fig. 3. A map of each geological unit in South Africa with the estimated background dose rate.

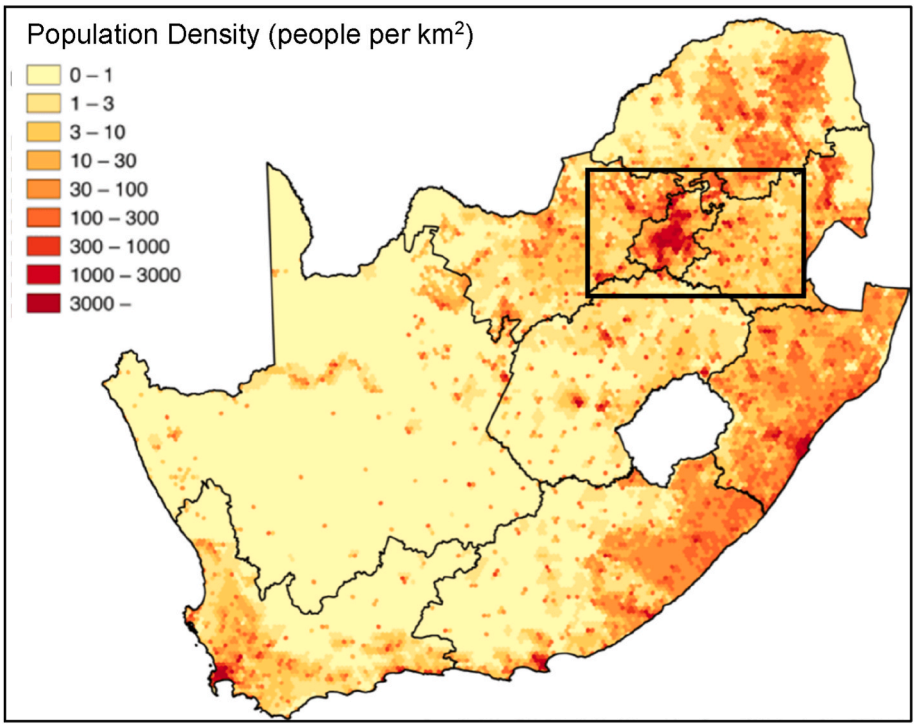

Fig. 4. A population density map of South Africa which indicates the most populous area in and around Gauteng with a black square (Frith, 2011).

za). Each geological unit was depicted as a polygon element in GIS format. The units were then populated with natural radionuclide concentrations. A differentiation was made between major and minor rock types in each unit. The typical geological dominance of rock types was considered when the major rock type within the unit was not indicated. The general approach was to select the radionuclide concentrations of the rock with the highest values in each unit or the rock that was considered to be dominant was chosen as representative.

4. Results

4.1. Estimating geothermal hotspots in South Africa due to naturally occurring radionuclide concentrations

The estimated Radioactive Heat Production (*RHP*) in μW/m^3 was calculated by applying the equation of Rybach (1988).

$$RHP = \rho(3.48\,A_K + 9.52\,A_U + 2.56\,A_{Th}) \times 10^{-5} \quad (1)$$

where 2.65 kg/m^3 was used as the average density (ρ) of rock (Sharma, 1997) and A_K, A_U and A_{Th} represented the potassium, uranium, and thorium, respectively. The weight of uranium, and thorium is expressed

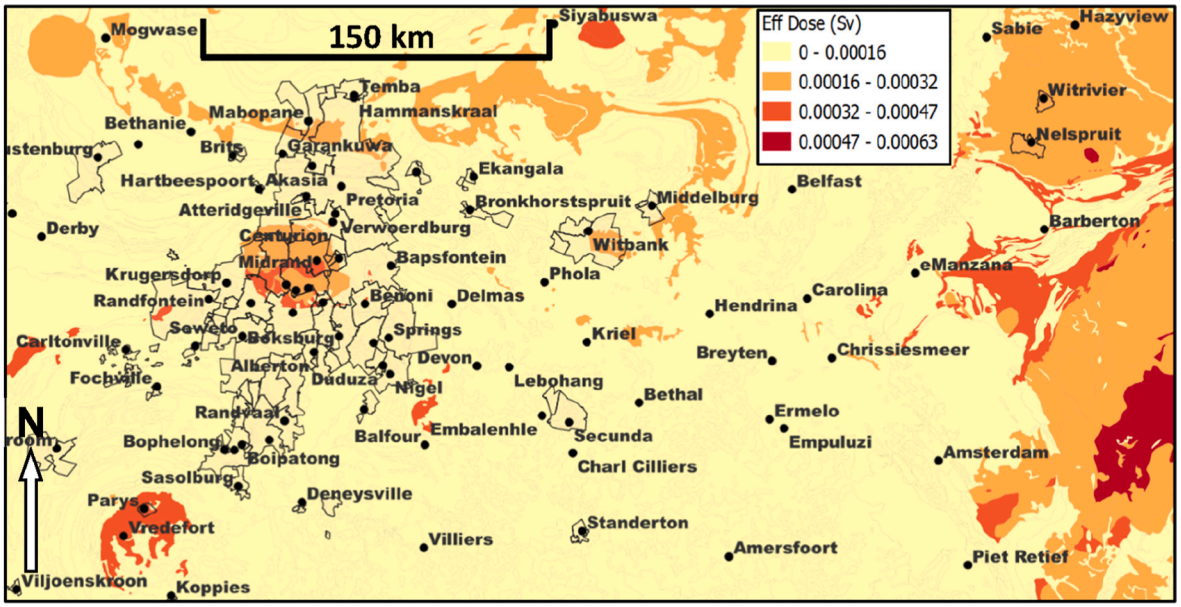

Fig. 5. A map of the central part of South Africa which is the most populous. The estimated annual effective dose is overlaid on the map.

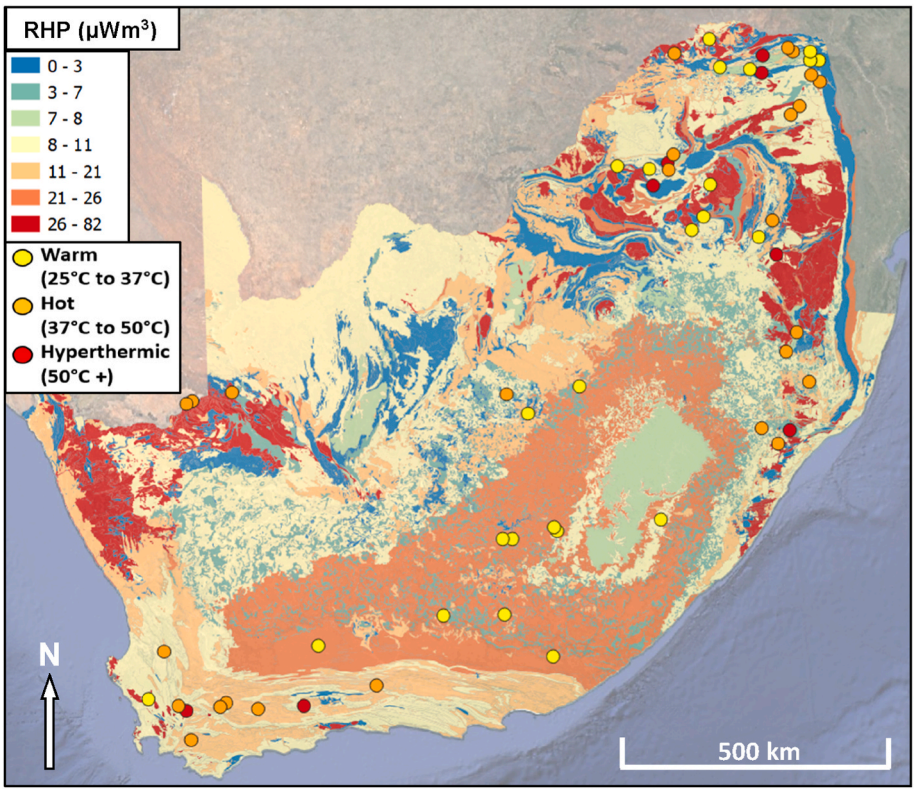

Fig. 6. An estimated radioactive heat production map overlaid by temperature graded points of the natural thermal springs in South Africa.

in ppm and potassium is in weight %. An equal quadrant colour index for the calculated radioactive heat production of each geological unit was then overlaid on a map of South Africa by using QGIS (Fig. 2).

4.2. Estimating terrestrial background radiation due to naturally occurring radionuclide concentrations

The background dose rates 1 m above the ground were estimated by combining the nuclide concentrations in each geological rock unit. The estimated dose rate (D) in nGy/h for each unit was calculated by (UNSCEAR, 2000)

$$D = 0.042\,A_K + 0.462\,A_U + 0.604\,A_{Th} \quad (2)$$

where A_K, A_U and A_{Th} represent the potassium, uranium, and thorium concentrations in Bq/kg, respectively. The estimated background dose rates were then colour graded and overlaid on a map of South Africa (Fig. 3).

The annual effective dose in Sievert for adults was then estimated by (UNSCEAR, 2000)

$$Eff\ Dose = D \times 0.2 \times 0.7 \times 24 \times 365 \quad (3)$$

where it was estimated that an average of 20% of time was spent outdoors (UNSCEAR, 2000), 0.7 Sv/Gy was used as the conversion factor from absorbed to effective dose and the other constants transformed from hours to years. These estimated annual effective doses were then overlaid on a map of Gauteng, which is the most populous part of South Africa, and the surrounding areas (Fig. 5). All the overlays were done using QGIS. Fig. 4 show the population density in South Africa as well as the area which was investigated.

5. Discussion

The estimated radioactive heat production map of South Africa (Fig. 2) shows levels higher than 26μW/m^3 in large areas of the far northeast and the far northwest. The high heat production areas in the far northeast comprises of the Limpopo Belt, the Bushveld Complex and the Barberton Greenstone Belt, all dominated by metamorphic, intrusive, and extrusive rock units. Smaller areas of high radioactive heat production are also evident in the Witwatersrand Basin and the Vredefort Dome, where the latter is also characterised by intrusions of granodiorites and granites.

The Namaqua Natal Belt area in the far northwest show levels higher than 26 μW/m^3 of heat production and a similar trend is evident in the far eastern coastal areas where the belt is exposed due to weathering of the Karoo Supergroup. All the large areas with high heat production (larger than 21 μW/m^3) in South Africa, apart from the Bushveld Complex, is related to weathering of overlaying geological groups and the consequent exposure of transboundary belts. The exposed granite bedrock in the Western and Southern Cape also give rise to similar areas with heat production higher than 26 μW/m^3. Radioactive heat production higher than 11 μW/m^3 was estimated for the Karoo Supergroup in the centre and the Cape Folded Belt in the south (Fig. 2). These formations are mainly sedimentary in origin.

A comparison was then made by overlaying the natural thermal springs (Jonker et al., 2013) on the estimated radioactive heat production map of South Africa (Fig. 6). The thermal springs were classified according to water temperature as warm (25 °C–37 °C), hot (37 °C–50 °C) and hyperthermic (hotter than 50 °C). Faults, folds, and dykes in geological structures were found to be associated with all the thermal springs in South Africa (Kent, 1969). Several of the thermal springs lay on the boundaries of the Namaqua Natal, Barberton Greenstone, and Limpopo mobile belts. These belts are dominated by igneous and metamorphic rock units with high concentrations of radionuclides. The largest number of thermal springs were found in the Limpopo Belt. These springs were classified as warm, hot and hyperthermic and are all characterised by half graben structures which faults and forms artesian springs (Olivier and Jonker, 2013). Warm, hot and two hyperthermic thermal springs are also located in the Bushveld Complex where high

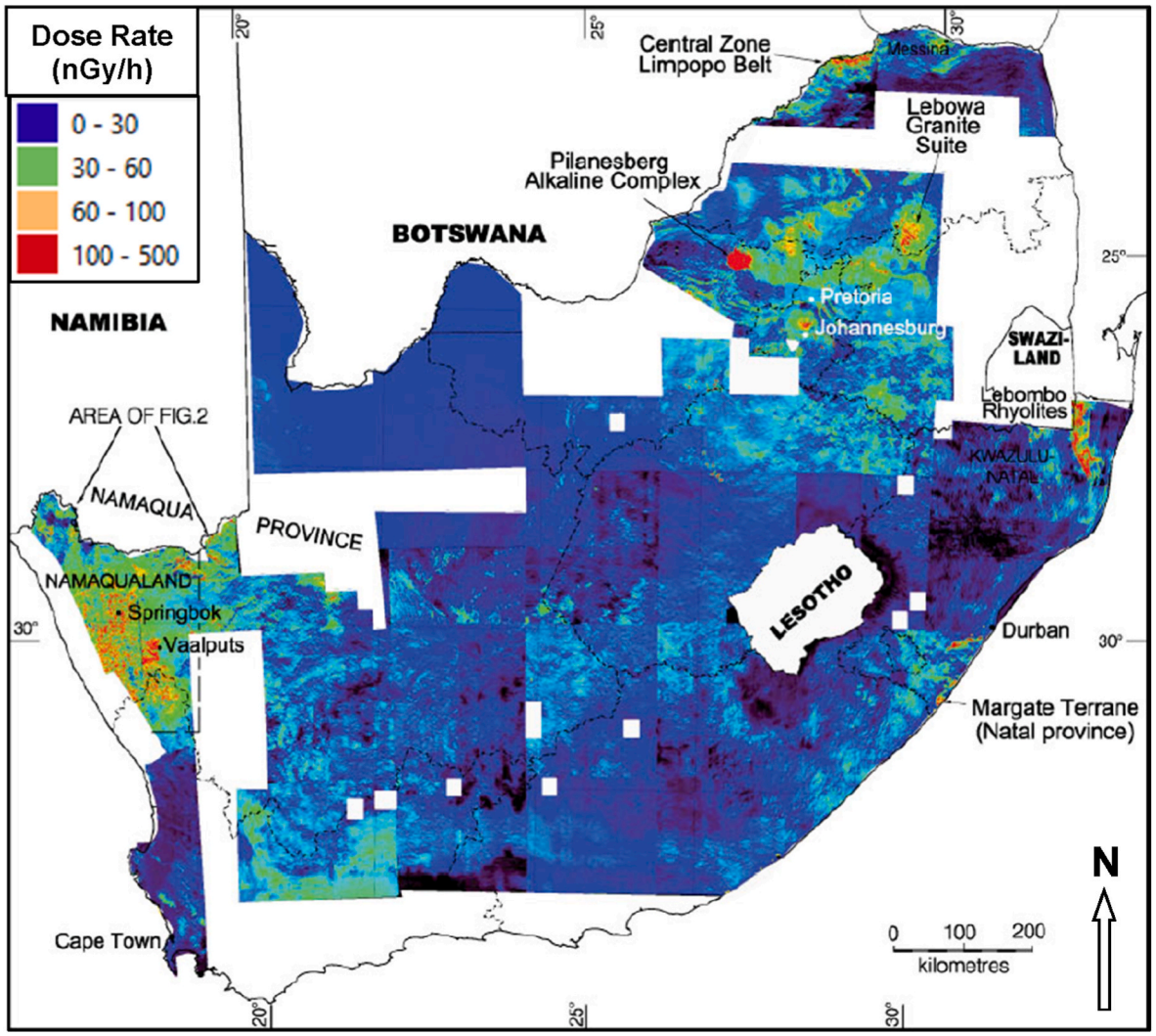

Fig. 7. Gamma ray exposure rate map of South Africa that was produced by combining measurements that was taken over a 30-year period (Andreoli et al., 2006).

heat production was estimated.

The Western Cape has a high number of hot and two hyperthermic thermal springs. These springs are associated with the folds and thrusts of the Cape Fold Belt and the Cape Granite Suite basement rock. Medium radioactive heat production was estimated in the Karoo Supergroup which is dominated by sedimentary and some extrusive, and intrusive rocks. This area consequently has several warm thermal springs (Fig. 6). The Namaqua Natal Metamorphic and Igneous Province gave rise to thermal springs both in the west and east of South Africa. Igneous rock units generally have higher heat production due to elevated nuclide concentrations when compared to metamorphic and sedimentary units. Carte and van Rooyen (1969) however demonstrated that metamorphic rock units have the highest thermal conductivity which can also influence thermal spring formation and water temperature. In light of this, the predicted nuclide heat production map of South Africa is strongly supported by the general spatial distribution and water temperature characteristics of the thermal springs.

Andreoli et al. (2006) assembled a background gamma dose rate map of South Africa by combining in situ measurements that were taken over a period of at least 30 years. These surveys were done with different types of equipment and protocols. The map covered nearly 80% of South Africa and is shown in Fig. 7 with a colour graded overlay. The map clearly demonstrates high gamma dose rates in the Bushveld Complex and the Namaqua Natal and Limpopo mobile belts. The Pilanesberg Alkaline Complex and the Midrand between Pretoria and Johannesburg show very high (higher than 100 nGy/h) background levels and the Karoo in the south show medium levels (30–60 nGy/h). A good visual corelation was found between the map which was produced by in situ measurements (Fig. 7) and the estimated background dose map in Fig. 3, which was extracted from nuclide concentrations in rock units.

Table 2
In situ measurements and geological constructed estimates of background dose rate for several towns in South Africa.

Town	In situ measurement (nG/h)	Estimated background dose rate (nG/h)
Springbok	>100	>200
Cape Town	0–30	0–50
Midrand	>100	>200
Durban	0–30	0–50
Margate	0–100	0–100
Messina	30–60	0–100
Pilanesberg	>100	>200

A quantitative assessment was also done by comparing the in situ measurements and the estimated background dose rates of several towns. These values are tabulated in Table 2, and it is evident that the in situ measurements support the results of the geological based estimates of the background dose rate.

A map of the effective dose per annum for the central part of South Africa is shown in Fig. 5. The high levels in the east of the map are due to

the exposed rocks of the Barberton Greenstone Belt and large formal developments like Witrivier and Nelspruit are found in this area. High effective dose per annum levels are visible in the Pilanesberg Alkaline Complex next to the town of Mogwase, the Midrand and the Vredefort Dome in the east on the map. The Midrand is a very densely populated suburb of the Witwatersrand. All the effective dose per annum levels is however well below the levels of terrestrial sources of 0.48 mSv per annum as listed by UNSCEAR (2000). This is also generally true for all the other areas where high effective dose per annum levels were estimated.

6. Conclusions

The areas in South Africa with high estimated radioactive heat production were mainly confined to transboundary belts, igneous intrusions, and other geological structures with metamorphic, intrusive, and extrusive rock units. The spatial distribution and water temperature of the thermal springs in South Africa also correlated well with the predicted high heat production areas. The map with the estimated background radiation shows a very good corelation with actual in situ measurements. No areas were found with dangerously high (higher that 20 mSv/y) effective dose per annum levels (Hendry et al., 2009).

The good agreement between the estimated maps and empirical data supported the methods of this study. The theoretical approach in this research by which GIS is applied to populate geology with nuclide concentrations provided important information on exposure and potential geothermal energy generation. This cost-effective estimation method can therefore also be applied to other areas of the globe. This can then be followed by focused fieldwork measurements of hotspots. This method can further be improved by refining the nuclide concentrations in rock units where various rock types occur.

Declaration of competing interest

The authors declare that they have no known competing financial interests or personal relationships that could have appeared to influence the work reported in this paper.

Data availability

Data will be made available on request.

References

Andreoli, M.A.G., Hart, R.J., Ashwal, L.D., Coetzee, H., 2006. Correlations between U, Th content and metamorphic grade in the western Namaqualand belt, South Africa, with implications for radioactive heating of the crust. J. Petrol. 47 (6), 1095–1118.

Bahnemann, K.P., 1973. The origin of the singelele granite gneiss, near Messina, northern Transvaal. Spec. Publ. Geol. Soc. S. Afr. 3, 235–244.

Bezuidenhout, J., 2013. Measuring naturally occurring uranium in soil and minerals by analysing the 352 keV gamma-ray peak of ^{214}Pb using a NaI(Tl)-detector. J. Appl. Radiat. Isotopes 80, 1–6.

Carte, A.E., Van Rooyen, A.I.M., 1969. Further Measurements of Heat Flow in South Africa. Geological Society. South Africa Special Publication No. . 2. Upper Mantle Symposium.

Chinoda, G., Moyce, W., Matura, N., Owen, R., 2009. Baseline Report on the Geology of the Limpopo Basin Area. Project WaterNet Zimbabwe.

Council of Geoscience of South African. Silverton. Pretoria. https://www.geoscience.org.za/images/DownloadableMaterial/RSA_Geology.pdf. (Accessed 1 February 2021).

Dickson, B.L., Scott, K.M., 1997. Interpretation of aerial gamma-ray surveys-adding the geochemical factors. J. Australian Geol. Geophy. 17, 187–200.

Fripp, R.E.P., 1983. The precambrian geology of the area around the sand river near Messina, central zone, Limpopo mobile belt. Spec. Publ. Geol. Soc. S. Afr. 8, 89–102.

Frith, A., 2011. Data from Census 2011 by Stats SA. https://census2011.adrianfrith.com/.

Ferreira, V.N., Silva, A.M., Toledo, C.L.B., Jácomo, M.H., de Assis, L.M., Pires, A.C.B., 2016. The use of alternative methods for differentiation of banded iron formations and iron ore in the body N4WS, Serra Norte – Carajás mineral province. Rev. Bras. Geofís. 34 (1), 65–94.

GEOROC database (Geochemistry of Rocks of the Oceans and Continents). Max planck institute for chemistry. Mainz, Germany. http://georoc.mpch-mainz.gwdg.de/georoc/. Updated 01/01/2021.

Hamilton, G.N.G., Finlay, J.G., 1928. Outline of Geology for South African Students. Central News Agency Ltd, Johannesburg. South Africa.

Harmsen, K., de Haan, F.A.M., 1980. Occurrence and behaviour of uranium and thorium in soil and water. Neth. J. Agric. Sci. 28, 40–62.

Hart, R.J., Moser, D., Andreoli, M., 1999. Archean age for the granulite facies metamorphism near the center of the Vredefort structure, South Africa. Geology 27, 1091–1094.

Hartnady, C.J.H., Joubert, P., Stowe, C.W., 1985. Proterozoic crustal evolution in southwestern Africa. Episodes 8, 236–244.

Hendry, J.H., Simon, S.L., Wojcik, A., Sohrabi, M., Burkart, W., Cardis, E., Laurier, D., Tirmarche, M., Hayata, I., 2009. Human exposure to high natural background radiation: what can it teach us about radiation risks? J. Radiol. Prot. 29 (2A).

Ielsch, M., Cuney, F., Buscail, F., Rossi, A., Leon, M.E., 2017. Cushing. Estimation and mapping of uranium content of geological units in France. J. Environ. Radioact. 166, 210–219.

Jonker, C.Z., van Ginkel, C., Olivier, J., 2013. Association between physical and geochemical characteristics of thermal springs and algal diversity in Limpopo Province, South Africa. WaterSA 39 (1).

Kent, L.E., 1969. The thermal waters in the Republic of South Africa. In: Proc. Of Symposium II on Mineral and Thermal Waters of the World, B-Overseas Countries, 19, Report of the 23rd Session of the International Geological Conference, 1968. Academia, Prague.

Lana, C., 2003. Geology and geochemistry of a granite-greenstone association in the south-eastern Vredefort dome, South Africa. S. Afr. J. Geol. 106 (4), p291–p314.

Lock, B.E., Paverd, A.L., Broderick, T.J., 1974. Stratigraphy of the Karroo volcanic rocks of the Barkly east district by transactions. of the Geological Society of South Africa 77, 117–129.

Maier, W.D., Barnes, S.J., Groves, D.I., 2013. The Bushveld Complex, South Africa: formation of platinum–palladium, chrome- and vanadium-rich layers via hydrodynamic sorting of a mobilized cumulate slurry in a large, relatively slowly cooling, subsiding magma chamber. Miner. Deposita 48, 1–56.

Mc Carthy, T., Rubidge, B., 2005. The Story of Earth and Life. EXXARO. Struik, Cape Town. www.random.struik.co.za.

Morgan, P., 1989. Heat flow in the earth. In: Geophysics. Encyclopedia of Earth Science. Springer, Boston.

Moore, J.M., 1989. A comparative study of metamorphosed supracrustal rocks from the western Namaqualand metamorphic complex. Bull. Precambrian Res. 37, 1–410. Unit.

Moore, J.M., Watkeys, M.K., Reid, D.L., 1990. The regional setting of the Aggenys/Gamsberg base metal deposits, Namaqualand, South Africa, 77–95. In: Spry, Bryndzia (Ed.), Regional Metamorphism of Ore Deposits.

Mira, H., El-Gharbawy, R.I., Elmowafy, A.A., Osman, A.F., El maadawy, W.M., 2020. Mineralogical and radiometric studies of granitic rocks in Wadi Sabbagh area, south Sinai, Egypt. IOP Conf. Ser. Mater. Sci. Eng. 975.

NCRP, 2015. National Council of radiation protection and measurements (NCRP) of the united sates environmental protection agency (EPA). Report 160.

Neumann, E., Svensen, H., Galerne, C.Y., Planke, S., 2011. Multistage evolution of dolerites in the Karoo large igneous province, Central South Africa. J. Petrol. 52 (5), 959–984.

Olson, J.C., Overstreet, W.C., 1964. Geologic distribution and resources of thorium. In: Geological Survey Bulletin 1204. Prepared Partly on Behalf of the U.S. Atomic Energy Commission.

Olivier, J., Jonker, N., 2013. Optimal utilisation of thermal springs in South Africa. Report to the water research commission. WRC Report No TT 577/13. South Africa.

Opiyo, A.S., 2009. Radioactivity and elemental analysis of carbonatite rocks from parts of Gwasi area, southwestern Kenya. In: Degree of Master of Science (Physics. of University of Nairobi, Kenya.

Rudnick, R.L., Gao, S., 2003. Composition of the continental crust. Treatise Geochem 3, 1–64.

Ruedas, T., 2017. Radioactive heat production of six geologically important nuclides. In: Technical Reports. American Geophysics Union. Data 10.1002/2017GC006997.

Ruffell, A., McKinley, J.M., Lloyd, C.D., Graham, C., 2006. Th/K and Th/U ratios from spectral gamma-ray surveys improve the mapped definition of subsurface structures. J. Environ. Eng. Geophys. 11 (1), 53–61.

Rybach, L., 1988. Determination of Heat Production Rate, Handbook of Terrestrial Heat-Flow Density Determination. Kluwer academic Publishers.

Shakotko, P.H., 2014. Paleoregolith and unconformity-type uranium mineralization at Beaverlodge lake, great bear magmatic zone, northwest territories. In: Master's Degree Thesis. University of Saskatchewan. Canada.

Sharma, P.V., 1997. Environmental and Engineering Geophysics. Cambridge University Press.

Shone, R., Booth, P., 2005. The Cape basin, South Africa: a review. J. Afr. Earth Sci. 43, 196–210.

Smithies, R.H., Marsh, J.S., 1996. Alkaline rocks in the Kuboos-Bremen igneous province, southern Namibia: the grootpenseiland and Marinkas Kwela complexes. Communications of the Geology Survey of Namibia 11.

Sohnge, P.G., Le Roex, H.D., Nel, H.J., 1948. The Geology of the Country Around Messina. An Explanation of Sheet No. 46 (Messina). South African Geological Survey, p. 82.

Sundal, A.V., Henriksen, H., Soldal, O., Strand, T., 2003. The influence of geological factors on indoor radon concentrations in Norway. Sci. Total Environ. 328 (1–3), 41–53.

Thomas, R.J., Agenbacht, A.L.D., Cornell, D.H., Moore, J.M., 1994. The late Kibaran of southern Africa: tectonic evolution and metallogeny. Ore Geol. Rev. 9, 131–160.

Tucker, R.F., Viljoen, R.P., Viljoen, M.J., 2016. A review of the Witwatersrand Basin - the World's greatest goldfield. Episodes 2, 105.

Tyler, A.N., 1994. Environmental Influences on Gamma Ray Spectrometry. Phd Thesis. University of Glasgow.
UNSCEAR, 2000. Sources and effects of ionizing radiation. In: U.N. Scientific Committee on Effects of Atomic Radiation, Report to the General Assembly, with Annexes. U.N.
Viljoen, M.J., 2015. The Mpumalanga/Limpopo escarpment: geology and fluvial landforms. In: Grab, S., Knight, J. (Eds.), Landscapes and Landforms of South Africa. Springer International Publications, Switzerland.
Zimmermann, U., Tait, J., Crowley, Q.G., Pashley, V., Straathof, G., 2011. The Witputs diamictite in southern Namibia and associated rocks: constraints for a global glaciation. Int. J. Earth Sci. 100, 511–526.